Article

A Study on the Variable Inductor Design by Switching the Main Paths and the Coupling Coils

Yen-Chung Chiang [1,*], Juo-Chen Chen [1,2] and Yu-Hsin Chang [3]

1   Department of Electrical Engineering, National Chung Hsing University, Taichung City 402202, Taiwan; juochen@ncut.edu.tw
2   Department of Electronic Engineering, National Chin-Yi University of Technology, Taichung City 411030, Taiwan
3   Department of Electronic Engineering, National Formosa University, Yunlin County 632301, Taiwan; yhchang@nfu.edu.tw
*   Correspondence: ycchiang1970@nchu.edu.tw

Abstract: In a radio frequency (RF) system, it is possible to use variable inductors for providing tunable or selective frequency range. Variable inductors can be implemented by the microelectromechanical system (MEMS) process or by using transistors as switches to change the routing of coils or coupling quantities. In this paper, we investigated the design method of a variable inductor by using MOS transistors to switch the main coil paths and the secondary coupled coils. We observed the effects of different metal layers, turn numbers, and layout arrangements for secondary-coupled coils and compared their characteristics on the inductances and quality factors. We implemented two chips in the 0.18 μm CMOS process technology for each kind of arrangement for verification. One inductor can achieve inductance values from about 300 pH to 550 pH, and the other is between 300 pH and 575 pH, corresponding to 59.3% and 62.5%, respectively, inductance variation range at 4 GHz frequency. Additionally, their fine step sizes of the switched inductances are from 0.5% to 6% for one design, and 1% to 12.5% for the other. We found that both designs achieved a large inductance tuning range and moderate inductance step sizes with a slight difference behavior on the inductance variation versus frequency.

Keywords: CMOS process technology; mutual coupling; quality (*Q*) factor; switches; variable inductor

1. Introduction

In radiofrequency (RF) applications, inductors and capacitors are usually used to form the load impedances, matching networks, etc. It is the trend that the RF front end concurrently supports different standards. For such a system, reconfigurable circuits and architectures will be required. For providing tunable or selective frequency ranges, switched capacitors or varactors are easier to design and implement, compared with variable inductors. However, ongoing efforts seek to design a suitable variable inductor. The most common method to design a variable inductor is the microelectromechanical system (MEMS) process [1–4]. Although these MEMS variable inductors may have good quality (*Q*) factors and higher self-resonance frequencies (SRF), with the ability of continuous tuning, they are difficult to integrate with other circuits that utilize the conventional CMOS process technologies.

Besides MEMS approaches, variable inductors can also be implemented by using transistors as switches to change routing paths of coils or coupling quantities. The simplest way is using CMOS transistors as switches to short or open an inductor that is in series with another inductor [5]. This method occupies a larger area for using two inductors, and the inductances can be changed by only two discrete values. Stacked multilayers [6] or proper routing [7] may resolve the area issue, but they can still not provide flexible inductance tuning. Another possible mechanism for changing the inductance is to vary

the mutual coupling between coils [8]. By switching the transistors on the secondary coupling loops, the mutual inductance between the main coil and the coupling coils will be changed; therefore, the resultant inductance of the main coil can be controlled. However, the inductance can still be switched as limited discrete values of large step sizes. The switching mutual inductance method is then extended to add some small coupling coils inside and outside of the main coils [9]. It can be shown that coarse steps of the inductance can be obtained by switching routing of main coils, and fine steps of the inductance can be obtained by switching the additional small coupling coils. Although this design seems to provide both coarse and fine-tuning of the inductance, we noticed that the fine-tuning step is too small to provide significant tuning in frequency, and large inductance gaps exist between coarse steps.

In this paper, we adopted a similar method as in [9] but used bottom metal layers to form the secondary coupling coils; thus, we can maximize the mutual coupling between the main coils and controlled coupling coils. We also tried multi-turns for the secondary coupling coils to investigate their influence on the inductance. The rest of this paper is structured as follows: Detailed design considerations are given in Section 2, and the experimental results are shown in Section 3. Finally, a simple conclusion is made in Section 4.

2. Variable Inductor Design

As mentioned in the previous section, a variable inductor can be realized by using CMOS transistors as switches to change the path of the main coils and/or the secondary coupling coils. Kossel et al. [9] proposed a variable inductor design adopting such a technique, both in main coils and secondary coupling coils. The authors sought to maximize the *Q*-factor of the secondary coupling coils; thus, they chose the thick top metal layer to implement both their main coils and secondary coupling coils. However, this choice limited the secondary coupling coils' area size, and all secondary coupling coils are of the one-turn path. Additionally, the resultant mutual coupling between the main coil and the secondary coupling coils is too small to provide significant inductance change. To maximize the overlapping area of the main coil and the secondary coupling coils, our efforts were to design the secondary coupling coils using the lower metal layers. The relation between the one-turn main coil and the one-turn secondary coupling coil has been comprehensively studied in the previous work [10]. Although the target of design in [8,10] is mainly to enlarge the inductance change, the analyses and equations provided in [10] still fit our secondary coupling coils design. However, the effects of different metal layers, turn numbers, and area sizes were not studied, and our target is to provide a moderate inductance step size. We first investigated the influence of different metal layers on mutual coupling. Then, we observed the difference of mutual coupling for the secondary coils being one turn or two turns. After these two investigations on the secondary coupling coils, we studied the influence of the area size of the secondary coupling coils. Then, we described the influence of the size of CMOS transistors and the design of main coils. All the simulations in this section were based on the 0.18 μm 1P6M CMOS process technology.

2.1. Influence of Metal Layer for Secondary Coupling Coil of One Turn

To investigate the mutual coupling for different metal layers of secondary coupling coil, we used a one-turn octagon shape at top metal (Metal 6) as the main coil and lower metal layer (Metal n; n = 1–5) to form the secondary coupling coil, as shown in Figure 1a. For our design purposes, the shape of the secondary coupling coil occupies approximately one-fourth of the main coil projection area. The width of the main coil is 15 μm, and the width of the secondary coupling coil is 9 μm. For each metal layer of the secondary coupling coil, we generated a similar layout and performed an electromagnetic (EM) simulation to obtain the mutual coupling between the two kinds of coils. The switch S_c in Figure 1a is set to be ideally short-circuited or ideally open-circuited to compare the difference of the inductance and the *Q* factor of the main coil. When S_c is open-circuited, the simulated main coil inductances are almost the same regardless of the metal layer used in the secondary

coupling coil. The simulated inductances under open-circuited S_c are about 534.6 pH, 547.1 pH, and 570 pH for 4 GHz, 8 GHz, and 12 GHz, respectively. The simulated Q factors under open-circuited S_c are about 10.88, 15.5, and 15.0 for 4 GHz, 8 GHz, and 12 GHz, respectively. Table 1 shows the simulated inductance changes in percentage and Q factors for different metal layers of secondary coupling coil under short-circuited switch S_c. Since the induced current in the secondary coupling coil is in the opposite direction according to Lenz's law, the mutual coupling between the main coil and the secondary coupling coil is negative, which causes a decrease in the inductance of the main coil. It can be seen that the mutual coupling increases as the secondary coupling coil is closer to the main coil for a higher metal layer. In the meantime, the Q factor also decreases as the secondary coupling coil is closer to the main coil. The relation between the inductance change and the Q factor is a trade-off.
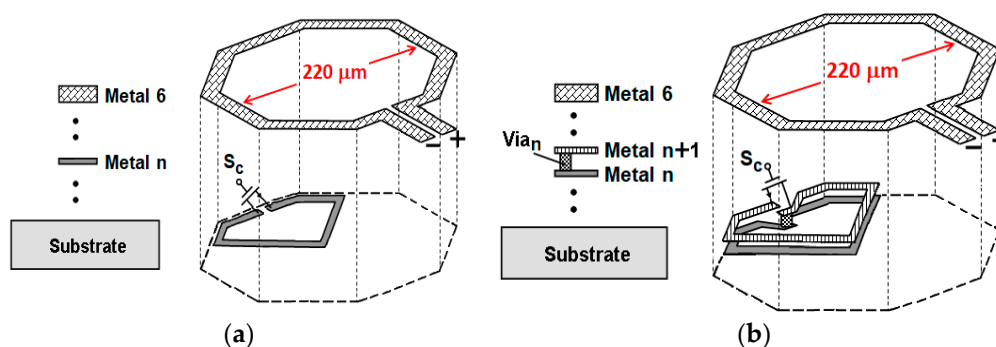

Figure 1. Three-dimensional illustration of variable inductors by switching secondary coupling coil: (**a**) one-turn secondary coupling coil and (**b**) two-turn secondary coupling coil.

Table 1. Simulated inductance changes in percentage and Q factors for different metal layers of secondary coupling coil under short-circuited switch S_c.

	Metal 1	Metal 2	Metal 3	Metal 4	Metal 5
L @ 4 GHz	−5.07%	−5.59%	−6.23%	−6.99%	−7.87%
Q @ 4 GHz	8.01	7.79	7.52	7.21	6.84
L @ 8 GHz	−6.37%	−7.06%	−7.84%	−8.84%	−10.08%
Q @ 8 GHz	11.87	11.55	11.14	10.64	10.01
L @ 12 GHz	−6.97%	−7.25%	−8.64%	−9.74%	−11.22%
Q @ 12 GHz	12.72	12.40	12.01	11.56	10.98

2.2. Influence of Metal Layer for Secondary Coupling Coil of Two Turns

To compare the mutual coupling for two-turn secondary coupling coils, we also used a one-turn octagon shape at top metal (Metal 6) as the main coil and lower metal layers (Metal n and n + 1; n = 1–4) to form the secondary coupling coil, as shown in Figure 1b. The geometry parameters are the same as those in Figure 1a, except for the secondary coupling coil occupying two bottom metal layers to form a two-turn coil. The switch S_c in Figure 1b is still set to be ideally short-circuited or ideally open-circuited, as in the previous subsection. When S_c is open-circuited, the simulated main coil inductances are almost the same regardless of the metal layer used in the secondary coupling coil. The simulated inductances under open-circuited S_c are about 527.9 pH, 540 pH, and 566 pH for 4 GHz, 8 GHz, and 12 GHz, respectively. The simulated Q factors under open-circuited S_c are about 10.9, 15.6, and 15.2 for 4 GHz, 8 GHz, and 12 GHz, respectively. Table 2 shows the simulated inductance changes in percentage and Q factors for different metal layers of secondary coupling coil under short-circuited switch S_c. There is still a trade-off between the inductance change and the Q factor. It can be found that the inductance change of the two-turn secondary coupling coil of metal n and n+1 is approximately 1.21 to 1.35 times

that of the one-turn case of metal n. The Q factor is better than the counterpart of the one-turn case.

Table 2. Simulated inductance changes in percentage and Q factors for different metal layers of two-turn secondary coupling coil under short-circuited switch S_c.

	Metal 1 and 2	Metal 2 and 3	Metal 3 and 4	Metal 4 and 5
L @ 4 GHz	−6.12%	−6.84%	−7.54%	−8.63%
Q @ 4 GHz	8.74	8.50	8.22	7.86
L @ 8 GHz	−7.28%	−8.94%	−9.02%	−10.52%
Q @ 8 GHz	13.35	13.0	12.59	12.00
L @ 12 GHz	−8.98%	−10.26%	−11.05%	−13.22%
Q @ 12 GHz	14.57	14.25	13.89	13.29

2.3. Influence of Area Size for Secondary Coupling Coil

To investigate the mutual coupling for different area sizes of the secondary coupling coil, we used a one-turn octagon shape at top metal (Metal 6) as the main coil and the most bottom metal layer (Metal 1) to form the secondary coupling coil, as shown in Figure 2a–d, which is similar to those in Section 2.1, but the secondary coupling coils occupies different area percentage from that in Figure 1a. The width of the main coil is still 15 μm, whereas the width of the secondary coupling coil is also 9 μm. Referring to Figure 2a–d, we simulated the percentages of 25%, 50% (not shown in Figure 2), 75%, 100%, and 150%. The simulated inductances under open-circuited S_c are the same as in Figure 1a and are about 534.6 pH, 547.1 pH, and 570 pH for 4 GHz, 8 GHz, and 12 GHz, respectively. The simulated Q factors under open-circuited S_c are about 10.88, 15.5, and 15.0 for 4 GHz, 8 GHz, and 12 GHz, respectively. Table 3 shows the simulated inductance changes in percentage and Q factors for different area percentages of secondary coupling coil under short-circuited switch S_c. It can be seen that the mutual coupling increases as the area of the secondary coupling coil increases, without exceeding the projection of the main coil area.
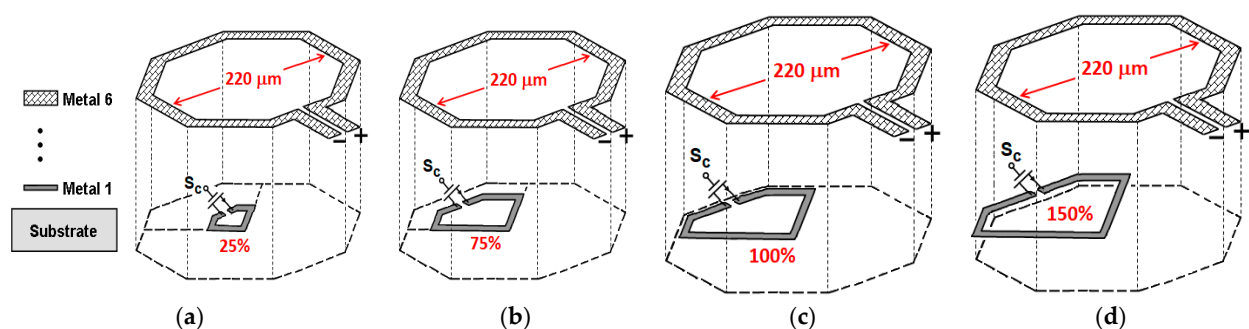

Figure 2. Three-dimensional illustration of variable inductors by switching secondary coupling coil that occupies different percentages of one-quarter of the projection area of the main coil: (**a**) 25%, (**b**) 75%, (**c**) 100%, and (**d**) 150% (exceeding the projection area).

Table 3. Simulated inductance changes in percentage and Q factors for different area percentages of one-turn secondary coupling coil under short-circuited switch S_c.

	25%	50%	75%	100%	150%
L @ 4 GHz	−0.27%	−1.14%	−3.25%	−5.07%	−1.73%
Q @ 4 GHz	10.62	9.83	8.77	8.01	9.75
L @ 8 GHz	−0.36%	−1.48%	−4.12%	−6.37%	−2.15%
Q @ 8 GHz	15.17	14.38	12.80	11.87	14.06
L @ 12 GHz	−0.42%	−1.62%	−4.47%	−6.97%	−2.32%
Q @ 12 GHz	14.77	14.25	13.13	12.72	14.01

In the meantime, the *Q* factor also decreases, as the overlapping area of the secondary coupling coil with the main coil is larger. From the case of 150%, the change in inductance will decrease because the secondary coupling coil encloses both the areas inside and outside of the projection of the main coil and the magnetic fields are opposite in direction for these two areas. The dependence of overlapping area on the change in inductance is a positive correlation but not with the proportion. Again, the relation between the inductance change and the *Q* factor is a trade-off.

2.4. Influence of Transister Size for Secondary Coupling Coil

In the previous simulations, we used an ideal short- or open-circuited design to investigate the effects of different metal layers, turn numbers, and area percentages of layout arrangement. In this subsection, we used the NMOS model in the simulation, in which the test geometry was as the arrangement shown in Figure 1b, and the two-turn secondary coupling coil was formed by metal 1 and 2, i.e., the most bottom two metal layers. The transistors were chosen to be NMOS with a channel length of 180 nm. From the summary shown in Table 4, it was found that both the inductance changes and *Q* factors increase as the NMOS sizes (W/L) increase. However, the SRF of the inductor also drops down significantly as the NMOS switches sizes increase. In the case of W = 300 μm case, the SRF drops to around 12 GHz, and this influences the inductance change percentage at that frequency. Therefore, we need to trade off the requirements of inductance tuning ability, *Q* factor, and SRF.

Table 4. Simulated inductance changes in percentage and *Q* factors for different widths of NMOS transistors as the switch of two-turn secondary coupling coil.

W	30 μm	60 μm	120 μm	180 μm	240 μm	300 μm
L @ 4 GHz	−1.63%	−3.20%	−4.61%	−5.25%	−5.60%	−5.85%
Q @ 4 GHz	8.04	8.01	8.04	8.16	8.26	8.32
L @ 8 GHz	−4.36%	−5.95%	−7.14%	−7.95%	−8.75%	−9.60%
Q @ 8 GHz	10.42	11.06	11.93	12.34	12.57	12.70
L @ 12 GHz	−6.89%	−8.34%	−10.90%	−13.92%	−14.88%	−3.81%
Q @ 12 GHz	11.13	12.28	13.19	13.54	13.73	13.84

2.5. Main Coil Design

For all the simulated cases we discussed above, the secondary coupling coils occupy only one-quarter of the projection area of the main coil. The largest percentage of inductance change is about 13%, which implies that the largest percentage of inductance change will not exceed 40% even if we fulfill the entire projection area with four similar secondary coupling coils. To extend the range of variable inductance, we also switched the paths of the main coil, as carried out in [9]. For the secondary coupling coils, although the single turn design using metal 5 or two-turn design using metals 4 and 5 have a larger percentage of inductance change, its SRF may be relatively low due to the small distance between metal layers 5 and 6. Therefore, we adopted a two-turn design by using metal 1 and 2 layers, which can provide acceptable fine-tuning inductance change with a better *Q* factor. The illustrations of the final two designs are shown in Figure 3a,b. In Figure 3a, we used three similar two-turn secondary coupling coils with a one-turn coil, and by changing the combination of the state of the switches S_{c1} to S_{c4}, we can obtain seven kinds of fine-tuned conditions. In addition, coarse tuning is achieved by switching the switches S_{m1} and S_{m2}, which can change the current paths in the main coils. The function of S_{m2} is relatively easy to understand in that it provides a shorter path and thus makes the inductance smaller if S_{m2} is short-circuited. The function of a turning-on switch S_{m1} is such that it can push the current distribution toward the center due to the proximity effect, and this also makes the inductance smaller. The design of Figure 3b is similar to that in Figure 3a except for the replacement of a two-turn secondary coupling coil with a smaller area rather than a

one-turn coil and for the positions of switches S_{m1} and S_{m2}. By switching both switches in main coils and secondary coupling coils, we can obtain coarse and fine-tuning of the inductance in the main coil. The mutual coupling by turning on S_{c2}–S_{c4} is almost the same, whereas the mutual coupling by turn-on S_{c1} is smaller than others. The effective turn number controlled by S_{c1} can be seen as one turn and S_{c2}–S_{c4} can be seen as two turns. By different combinations of the status of switches S_{c1}–S_{c4}, the effective turns (N_{eff}) of the secondary coupling coils can vary from 0 (all switches turned off) to 7 (all switches turned on). To maintain the operation of the main coil as a symmetrical inductor, switches S_{c2} and S_{c3} should be turned on or off simultaneously. With the proper controlling design of main coils and secondary coupling coils, the inductance can vary over a large range with moderate step size without a large gap of inductance value in the whole inductance range.
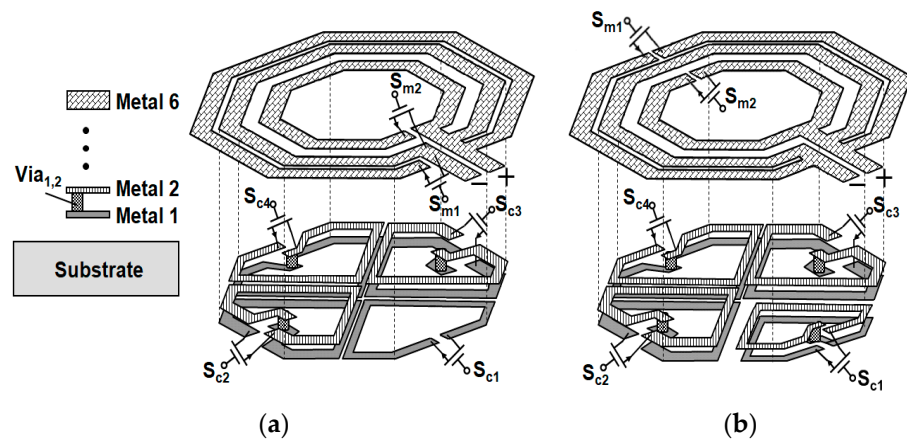

(a) **(b)**

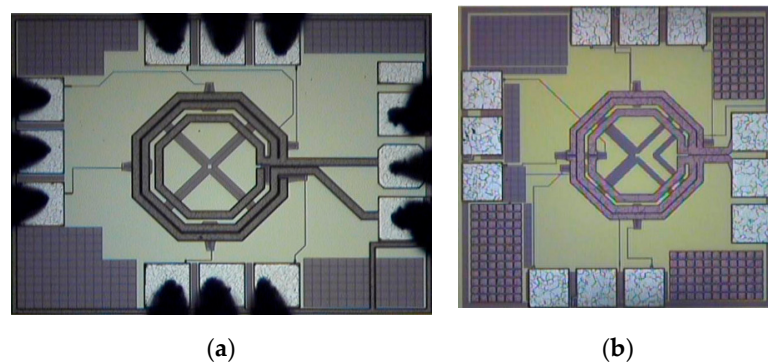**Figure 3.** Three-dimensional illustration of variable inductors by switching secondary coupling coil: (**a**) three one-quarter two-turn and one one-turn secondary coupling coils and (**b**) three one-quarter two-turn secondary coupling coils with one smaller two-turn coil.

The width of the main coils was chosen to be 15 μm. The inner radius of the inner, center, and outer paths of the main coils were 85 μm, 110 μm, and 127 μm, respectively. The width of the bottom secondary coupling coils was chosen to be 9 μm. We adopted NMOS transistors to implement the switches S_{m1}, S_{m2}, and S_{c1} to S_{c4}. The influence of the transistor size for S_{m1} and S_{m2} is similar to the discussion made in Section 2.4. The NMOS transistors of S_{m1} and S_{m2} were chosen to be 4 μm/180 nm × 50 fingers for the main coils, while the NMOS transistors of S_{c1}–S_{c4} were 5 μm/180 nm × 60 fingers for the bottom secondary coupling coils.

3. Experimental Results and Discussions

The proposed variable inductors were implemented in the 0.18 μm CMOS process technology. The micrographs of the proposed variable inductors are as shown in Figure 4a,b in which the chip sizes are 0.768 mm × 0.574 mm for the inductor in Figures 3a and 4a, and 0.686 mm × 0.620 mm for the inductor in Figures 3b and 4b. The s-parameter measurements for the proposed inductors were performed on the Agilent 8753ES network analyzer.

The simulated or measured resultant inductances were obtained by using the definition of the inductance: $L = \text{Im}(Z_{in})/\omega$ from s-parameters. Figure 5a–d shows the simulated inductances versus the frequencies of the proposed variable inductor in Figure 3a under different switch conditions for S_{m1} and S_{m2} in which "0" represents the OFF status, and "1" stands for the ON status. The eight curves in each subfigure represent the resultant inductances versus the frequencies for one of the eight possible combinations of S_{c1} to S_{c4} and the effective turns N_{eff} mentioned in the previous subsection, as shown in the inset of Figure 5d. The corresponding measured results are as shown in Figure 6a–d. It can be seen that the inductances have coarse change steps by switching the status of Sm1 and Sm2. Additionally, it can also be investigated that fine step size can be achieved by

switching the status of the secondary coupling coils. For the simulated results, the inductor has a peak inductance of 940 pH at 10.25 GHz for all switches being OFF and the lowest inductance of 255 pH at 9 GHz for all switches being ON. As for the measured case at the 4-GHz frequency, the largest inductance is 553 pH and the smallest inductance is 300 pH, corresponding to a change rate of the inductance of about 59.3%. Additionally, the fine step sizes of the switched inductances in Figure 6a–d are about 0.5% to 6.1% for most inductance range at 4 GHz. However, the frequency characteristic of the one-turn secondary coupling coil controlled by Sc1 has a slightly different trend, compared with the two-turn coils. Moreover, the inductances roll off for frequencies larger than 6 GHz due to additional parasitic capacitance and loss from switches.

(**a**) (**b**)

Figure 4. Micrographs of variable inductors by switching secondary coupling coil: (**a**) three one-quarter two-turn and one one-turn secondary coupling coils as in Figure 3a and (**b**) three one-quarter two-turn secondary coupling coils with one smaller two-turn coil as in Figure 3b.
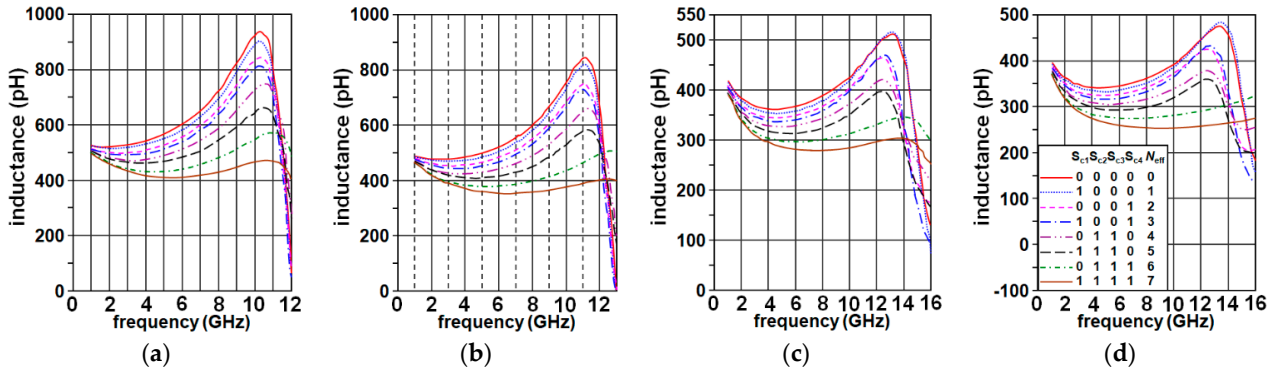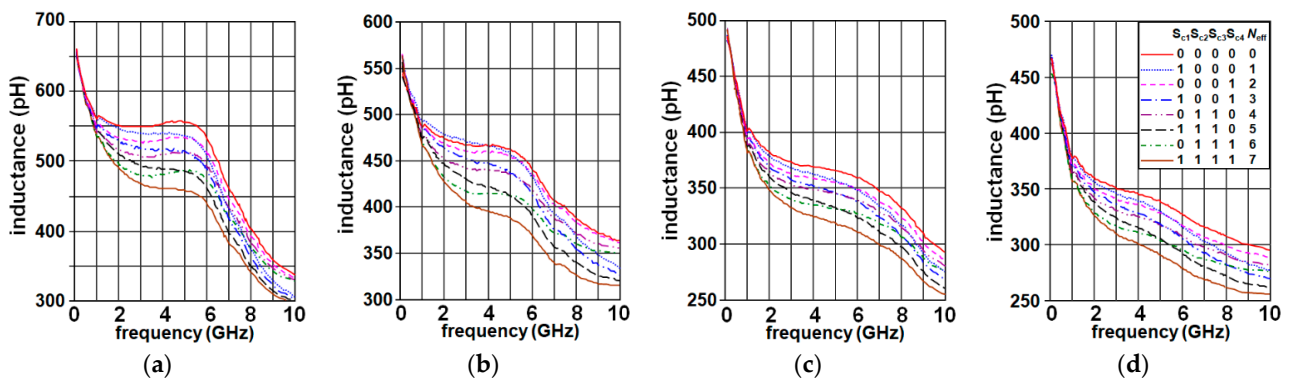

(**a**) (**b**) (**c**) (**d**)

Figure 5. Simulated inductances versus frequencies of the design in Figure 3a: (**a**) S_{m1} S_{m2} = "0 0", (**b**) S_{m1} S_{m2} = "1 0", (**c**) S_{m1} S_{m2} = "0 1", and (**d**) S_{m1} S_{m2} = "1 1".

(**a**) (**b**) (**c**) (**d**)

Figure 6. Measured inductances versus frequencies of the design in Figure 3a: (**a**) S_{m1} S_{m2} = "0 0", (**b**) S_{m1} S_{m2} = "1 0", (**c**) S_{m1} S_{m2} = "0 1", and (**d**) S_{m1} S_{m2} = "1 1".

Figures 7a–d and 8a–d show the corresponding simulated and measured Q factors versus the frequencies of the proposed inductor in Figure 3a and the eight curves in each subfigure are under the same control status as those in Figures 5a–d and 6a–d except for the quantities are changed as the Q factors. The simulated and measured Q factors are obtained from the simulated or measured s-parameters by using the definition $Q = \mathrm{Im}(Z_{in})/\mathrm{Re}(Z_{in})$. For the simulated results, it can be seen that the peaks of the Q factors occur at the frequency range from 4.1 GHz to 8.0 GHz depending on the status of the switches S_{m1} and S_{m2}. There is a highest peak Q factor of 6.6 at 4.1 GHz for all switches being OFF, and there is a lowest peak Q factor of 2.8 at 5 GHz for S_{m1} and S_{m2} being OFF and S_{c1}–S_{c4} being ON. As for the measured cases, it can be seen that the peaks of the Q factors occur at the frequency range from 2.0 GHz to 3.0 GHz for most of the cases which are obviously lower than the simulated ones. Additionally, the peak values of Q factors are from 2.8 to 4.7 depending on the status of switches. The values of Q factors are varied from 2.5 to 3.75 at the frequency of 4 GHz. Again, the frequency ranges of the measured Q factors are smaller than those obtained by simulation, and the values indicate that additional loss exists in real cases.
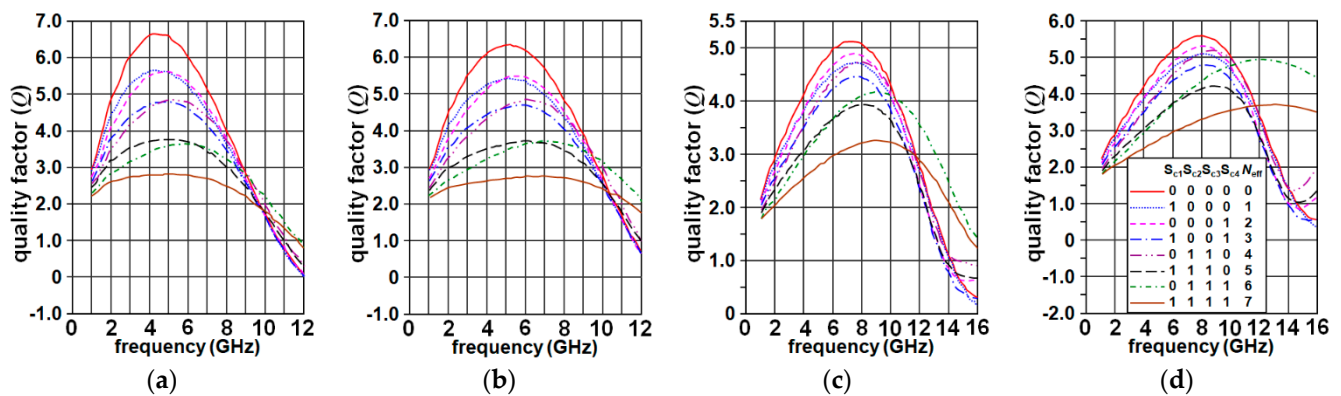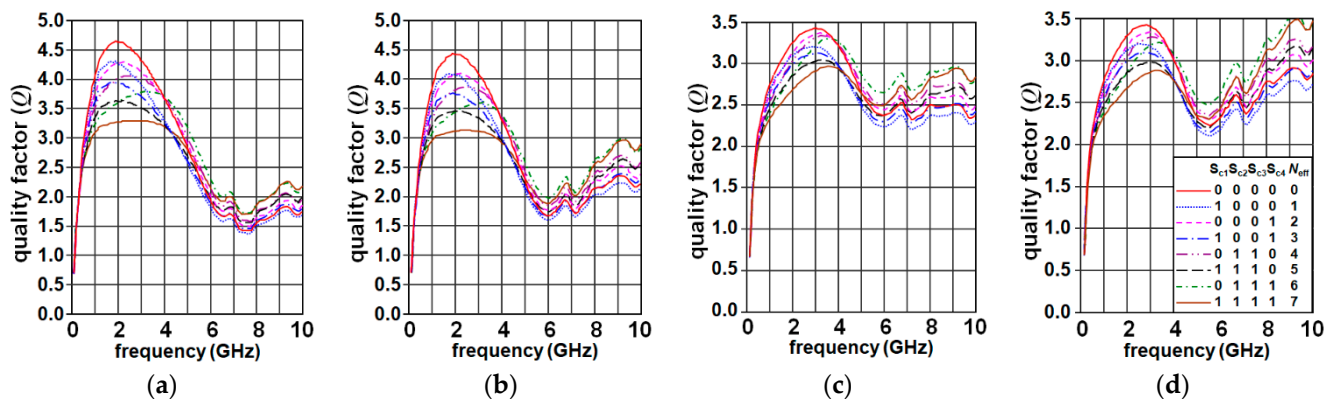

Figure 7. Simulated Q factors versus frequencies of the design in Figure 3a: (**a**) $S_{m1}\ S_{m2}$ = "0 0", (**b**) $S_{m1}\ S_{m2}$ = "1 0", (**c**) S_{m1} S_{m2} = "0 1", and (**d**) $S_{m1}\ S_{m2}$ = "1 1".

Figure 8. Measured Q factors versus frequencies of the design in Figure 3a: (**a**) $S_{m1}\ S_{m2}$ = "0 0", (**b**) $S_{m1}\ S_{m2}$ = "1 0", (**c**) S_{m1} S_{m2} = "0 1", and (**d**) $S_{m1}\ S_{m2}$ = "1 1".

Figures 9a–d and 10a–d show the simulated and measured inductances versus the frequencies of the proposed variable inductor in Figure 3b under different switch conditions for S_{m1}, S_{m2}, and S_{c1}–S_{c4}. The eight curves in each subfigure are similar to those in Figures 5–8. Again, it can be seen that the inductances have coarse change steps by switching the status of S_{m1} and S_{m2} and fine change steps by switching the status of S_{c1}–S_{c4}. The simulated results are very similar to those shown in Figure 5a–d. As for the measured ones, the results are more similar to the simulated results at the frequency range between 1 GHz

to 6 GHz for most cases, especially for the function of switch S_{c1}. At the 4 GHz frequency, the largest inductance is 575 pH, and the smallest inductance is 300 pH, corresponding to a change rate of the inductance of about 62.5%. Additionally, the fine step sizes of the switched inductances in Figure 10a–d are about 1% to 12.5% for most inductance range at 4 GHz. Again, the inductances show higher-order component behavior for frequencies larger than 6 GHz due to additional parasitic capacitance and loss from switches.
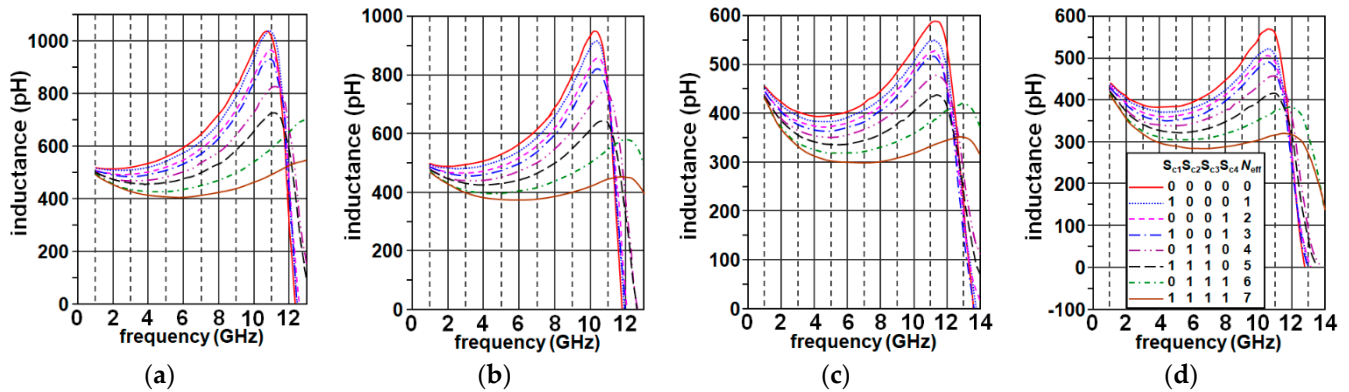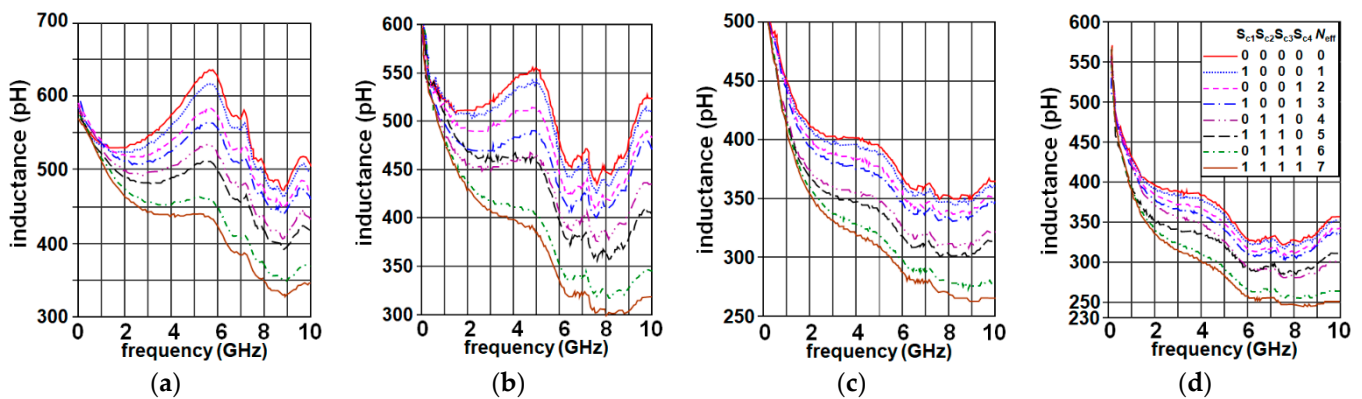

Figure 9. Simulated inductances versus frequencies of the design in Figure 3b: (**a**) S_{m1} S_{m2} = "0 0", (**b**) S_{m1} S_{m2} = "1 0", (**c**) S_{m1} S_{m2} = "0 1", and (**d**) S_{m1} S_{m2} = "1 1".

Figure 10. Measured inductances versus frequencies of the design in Figure 3b: (**a**) S_{m1} S_{m2} = "0 0", (**b**) S_{m1} S_{m2} = "1 0", (**c**) S_{m1} S_{m2} = "0 1", and (**d**) S_{m1} S_{m2} = "1 1".

Figures 11a–d and 12a–d show the corresponding simulated and measured Q factors versus the frequencies of the proposed inductor in Figure 3b, and the eight curves in each subfigure are under the same control status as those in Figures 9a–d and 10a–d, except for the quantities are changed as the Q factors. For the simulated results, it can be seen that the peaks of the Q factors occur at the frequency range from 4.2 GHz to 6.0 GHz, depending on the status of the switches S_{m1} and S_{m2}. There is a highest peak Q factor of 7.95 at 4.2 GHz for all switches being OFF, and there is a lowest peak Q factor of 2.6 at 7 GHz for all switches being ON. As for the measured cases, it can be seen that the peaks of the Q factors occur at the frequency range from 3.3 GHz to 4.5 GHz for most of the cases. Additionally, the peak values of Q factors are from 1.45 to 5.9 depending on the status of switches. The values of Q factors are varied from 1.45 to 5.65 at the frequency of 4 GHz. The loss on the switches seems to be worse than the case in Figure 3a for most cases except for the case in which all switches are in OFF status or only the switch S_{c1} is ON.
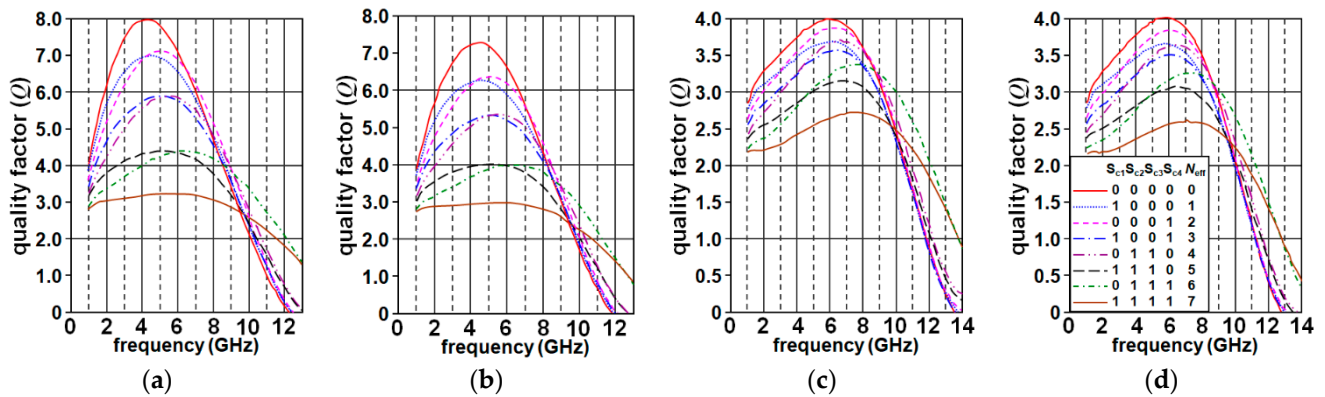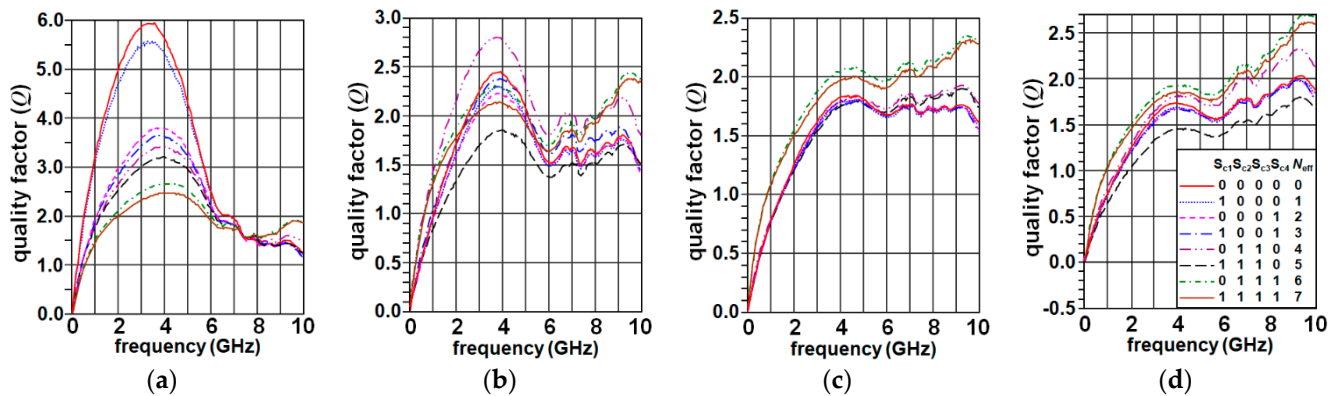
Figure 11. Simulated *Q* factors versus frequencies of the design in Figure 3b: (**a**) S_{m1} S_{m2} = "0 0", (**b**) S_{m1} S_{m2} = "1 0", (**c**) S_{m1} S_{m2} = "0 1", and (**d**) S_{m1} S_{m2} = "1 1".

Figure 12. Measured *Q* factors versus frequencies of the design in Figure 3b: (**a**) S_{m1} S_{m2} = "0 0", (**b**) S_{m1} S_{m2} = "1 0", (**c**) S_{m1} S_{m2} = "0 1", and (**d**) S_{m1} S_{m2} = "1 1".

In the design shown in Figure 3a, we aimed to combine two-turn secondary coupling coils with a one-turn coil for flexible tuning. We knew from Sections 2.1 and 2.2 that the inductance changes of the two-turn secondary coupling coil of metal 1 and 2 are approximately 1.21 to 1.28 times that of the one-turn case of metal 1. Since each of the secondary coupling coils occupied one-quarter of the projection area of the main coil, no matter one turn or two turns, we expected the inductance change of m two-turn coils plus 1 one-turn coil will tend to the inductance change of (m+1) two-turn coils. However, the results shown in Figure 6a–d point to a different trend: the inductance change of m two-turn coils plus 1 one-turn coil tends to the inductance change of (m+1) two-turn coils at low frequency but tends to be m two-turn coils at a higher frequency. This may be due to the mutual coupling behavior difference between two-turn and one-turn secondary coupling coils, and it may also have the influence of the difference in the parasitic capacitance and resistance for the two cases. Nevertheless, this combination cannot provide uniform inductance change over a range of frequencies, and this may limit its application.

On the other hand, the combination of coils with different area sizes of two-turn secondary coupling coils can provide a relatively uniform inductance change over a range of frequencies. However, the step sizes of inductance changes become nonuniform between different N_{eff} combinations for S_{m1} or S_{m2} that have ON status. This may be due to the current distribution of the main coil changed by switches S_{m1} and S_{m2}, and the effective coupling areas are also changed from the original expected.

For investigating the step size of each switching status, we also calculated the differential nonlinearity (*DNL*) for each designed variable inductor from the measured data. The *DNL* is defined as

$$DNL = \frac{L(N_{eff}+1) - L(N_{eff})}{\Delta L(LSB)} - 1,$$ (1)

in which $L(LSB)$ is defined as

$$\Delta L(LSB) = \frac{L(N_{eff}=0) - L(N_{eff}=7)}{7},$$ (2)

i.e., the uniform inductance changing step size by switching S_{c1}–S_{c4} for a certain S_{m1} S_{m2} status. The calculated *DNL* for the variable inductors shown in Figure 3a,b, respectively, are shown in Figure 13a,b, respectively. It can be seen that DNLs are within ±0.5 for most cases and the DNLs of the design in Figure 3b are averagely smaller than that of the design in Figure 3a except for some switching status. These results can be explained by the discussion provided in the previous two paragraphs.
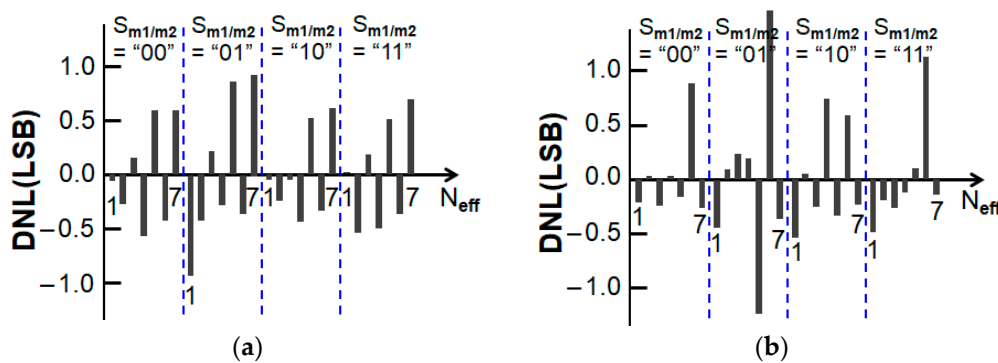

Figure 13. Measured DNL of variable inductors for case: (**a**) three one-quarter two-turn and one one-turn secondary coupling coils, as in Figure 3a, and (**b**) three one-quarter two-turn secondary coupling coils with one smaller two-turn coil, as in Figure 3b.

From the results in previous work [9], we observed that the *Q* factor dropped significantly as the switches turned on, and this also happened in our cases. This effect is especially obvious in the results shown in Figure 12a–d. For the case that all switches are off, the *Q* factor has a peak value of 5.95 at 3.4 GHz. As S_{c1} turns on, the peak of *Q* factor drops to about 5.5. For all other cases, *Q* factors do not exceed 3.85. The switches on the main coil paths will directly consume the power flowing in the path. The switches on the secondary coupling will decrease the magnetic energy store in the whole structure, and the parasitic resistance in the transistor also consumes power, which makes the *Q* factor even worse. Although a larger size of switch transistor may alleviate the loss, the parasitic capacitance will make the SRF significantly drop down. Besides the factors discussed above, another reason for the difference between the simulated results and the measured ones may be the NMOS model. Since we used the RF-NMOS, which has a fixed layout, and the parasitic effects are included in the device model, we did not include the layout of the NMOS at the EM stage. However, the metal layers of the NOMS transistors are located just beneath the designed coils, and there must be parasitic capacitance between them. The additional parasitic may further limit the bandwidth and *Q* factor of the designed variable inductor.

In our design, there are two sub-coils controlled by S_{m1} and S_{m2}. This design is to prevent a large gap of inductance change. From the results shown above, the inductance change caused by the outer main coil controlled by S_{m1} is relatively small, but it introduces significant parasitic capacitance and resistance. Therefore, the path controlled by S_{m1} can be omitted to improve the bandwidth and the *Q* factor. Another strategy to improve the

performance of the variable inductor may use the one-turn secondary coupling coils at the upper metal layers.

4. Conclusions

In this paper, we demonstrated a variable inductor design method using NMOS transistors as switches to change the main coil paths and secondary coupling coils. By changing the status of switches in both types of coils, large inductance tuning ranges with moderate step sizes are achieved. We successfully fabricated two chips of variable inductors. These variable inductors were designed and implemented in the 0.18 μm CMOS process technology. The proposed variable inductors can achieve 59.3% and 62.5%, respectively; inductance variation ranges and the fine step sizes of the switched inductances are about 0.5% to 6.1% for one design and 1% to 12.5% for the other for most inductance ranges at 4 GHz frequency. The *Q* factor property limits the application of the variable inductor, and it needs to be improved in future work. However, this variable inductor can still be used in some applications such as a wideband amplifier or wideband injection-locked frequency divider in which the *Q* factor may not be so critical.

References

1. Lubecke, V.M.; Barber, B.; Chan, E.; Lopez, D.; Gross, M.E.; Gammel, P. Self-assembling MEMS variable and fixed RF inductors. *IEEE Trans. Microw. Theory Tech.* **2001**, *49*, 45–50. [CrossRef]
2. Yokoyama, Y.; Fukushige, T.; Hata, S.; Masu, K.; Shimokohbe, A. On-chip variable inductor using microelectro-mechanical systems technology. *Jpn. J. Appl. Phys.* **2003**, *42*, 2190–2192. [CrossRef]
3. Chang, S.; Sivoththaman, S. A tunable RF MEMS inductor on silicon incorporating an amorphous silicon bimorph in a low-temperature process. *IEEE Electron Device Lett.* **2006**, *27*, 905–907. [CrossRef]
4. Gmati, I.E.; Calmon, P.F.; Boukabache, A.; Pons, P.; Fulcrand, R.; Pinon, S.; Boussetta, H.; Kallala, M.A.; Besbes, K. Fabrication and evaluation of an on-chip liquid micro-variable inductor. *J. Micromech. Microeng.* **2011**, *21*, 1–9. [CrossRef]
5. Li, Z.; Quintal, R. A dual-band CMOS front-end with two gain modes. *IEEE J. Solid-State Circuits* **2004**, *39*, 2069–2073.
6. Park, P.; Kim, C.S.; Park, M.Y.; Kim, S.D.; Yu, H.K. Variable inductance multilayer inductor with MOSFET switch control. *IEEE Electron Device Lett.* **2004**, *25*, 144–146. [CrossRef]
7. Sadhu, B.; Kim, J.; Harjani, R. A CMOS 3.3–8.4 GHz wide tuning range, low phase noise LC VCO. In Proceedings of the IEEE Custom Integrated Circuits Conference, San Jose, CA, USA, 13–16 September 2009; pp. 559–562.
8. Demirkan, M.; Bruss, S.P.; Spencer, R.R. 11.8 GHz CMOS VCO with 62% tuning range using switched. In Proceedings of the IEEE Radio Frequency Integrated Circuits Symposium, Honolulu, HI, USA, 3–5 June 2007; pp. 401–404.
9. Kossel, M.; Morf, T.; Buchmann, P.; Schmatz, M.L.; Menolfi, C.; Toifl, T. Switched inductor with wide tuning range and small inductance step sizes. *IEEE Microw. Wireless Compon. Lett.* **2009**, *19*, 515–517. [CrossRef]
10. Demirkan, M.; Bruss, S.P.; Spencer, R.R. Design of wide tuning-range CMOS VCOs using switched coupled-inductors. *IEEE J. Solid-State Circuits* **2008**, *43*, 1156–1163. [CrossRef]